

DiffusePast: Diffusion-based Generative Replay for Class Incremental Semantic Segmentation

Jingfan Chen^{1,2}, Yuxi Wang^{†2,3,4}, Pengfei Wang^{1,2}, Xiao Chen^{1,2},
 Zhaoxiang Zhang^{†2,3,4}, Zhen Lei^{†2,3,4}, and Qing Li^{†1}

¹The Hong Kong Polytechnic University

²Center for Artificial Intelligence and Robotics, HKISI, CAS

³Institute of Automation, Chinese Academy of Sciences

⁴University of Chinese Academy of Sciences

jingfan.chen@connect.polyu.hk

Abstract

The Class Incremental Semantic Segmentation (CISS) extends the traditional segmentation task by incrementally learning newly added classes. Previous work has introduced generative replay, which involves replaying old class samples generated from a pre-trained GAN, to address the issues of catastrophic forgetting and privacy concerns. However, the generated images lack semantic precision and exhibit out-of-distribution characteristics, resulting in inaccurate masks that further degrade the segmentation performance. To tackle these challenges, we propose DiffusePast, a novel framework featuring a diffusion-based generative replay module that generates semantically accurate images with more reliable masks guided by different instructions (*e.g.*, *text prompts or edge maps*). Specifically, DiffusePast introduces a dual-generator paradigm, which focuses on generating old class images that align with the distribution of downstream datasets while preserving the structure and layout of the original images, enabling more precise masks. To adapt to the novel visual concepts of newly added classes continuously, we incorporate class-wise token embedding when updating the dual-generator. Moreover, we assign adequate pseudo-labels of old classes to the background pixels in the new step images, further mitigating the forgetting of previously learned knowledge. Through comprehensive experiments, our method demonstrates competitive performance across mainstream benchmarks, striking a better balance between the performance of old and novel classes.

1 Introduction

Deep learning has revolutionized various domains by leveraging large pre-collected datasets for training and achieving human-level performance [14, 21, 34, 35]. However, real-world scenarios often involve data streams with storage and privacy constraints, requiring Class-Incremental Learning (CIL) for incremental model updates with new class instances [38, 24, 20, 49]. CIL typically faces the challenge of *catastrophic forgetting*, which results in the degradation of performance for old classes as new classes are learned. This issue is more severe in complex tasks like class incremental semantic segmentation (CISS), as recent works emphasize [6, 12, 7].

Most existing CISS methods employ the regularization-based methods [6, 7, 31, 2], which aim to alleviate the aforementioned challenges through calibrated loss functions. In addition, replay-based

[†] Equally advising corresponding authors. E-mails: yuxiwang93@gmail.com, zhaoxiang.zhang@ia.ac.cn, zlei@nlpr.ia.ac.cn, csqli@comp.polyu.edu.hk

approaches [7, 31, 2] offer a complementary solution by replaying a small number of samples from previous steps to retain old class knowledge. This technique is commonly referred to as *memory replay* and serves to mitigate catastrophic forgetting. Although demonstrated to be effective, memory replay is limited by privacy concerns (i.e., the access restrictions of previous step images [8, 10]) and the collected samples may not fully capture the diverse semantics within each class. To alleviate these problems, *generative replay*-based method [26] replays old class images produced from a Generative Adversarial Network (GAN) [17] pre-trained on ImageNet [11]. Specifically, this method generate replayed images and use the previous step’s model to provide corresponding pseudo-labels. Consequently, the quality of the generated images and pseudo-labels plays a crucial role in CISS performance.

However, this GAN-based method encounters two issues that lead to a decline in the quality of generated images and pseudo-labels, as shown in Figure 1. Firstly, it generates **semantically inaccurate** images (e.g., producing a horsecart instead of a horse). This issue arises from an out-of-vocabulary problem, where the horse category is not present in the ImageNet dataset used to train the GAN. Secondly, even when semantically accurate images are generated, there can be a **distribution mismatch** between the generated images and the original training data (e.g., generating images with different styles) due to the frozen generator as depicted in [26]. Consequently, this distribution gap can lead to imprecise pseudo-labels. These two issues, affecting the quality of generated images and pseudo-labels, ultimately contribute to a decline in the overall performance of CISS.

To address these problems, this paper introduces a novel framework named DiffusePast, which integrates a diffusion-based generative replay module. This module leverages the capabilities of pre-trained Stable Diffusion [36] to generate semantically accurate images for replay. To enhance the precision of pseudo-labels, we propose a novel dual-generator paradigm consisting of *Distribution-aligned Diffusion Replay* (DDR) and *Structure-preserved Diffusion Replay* (SDR), as shown in Figure 1. Specifically, DDR focuses on generating images that share a similar distribution with the old class training data, improving the reliability of the generated pseudo masks. On the other hand, SDR aims to preserve the semantic structure of the original images from the previous step. For example, it generates new chair images with the same structure (layout) as the original chair images, allowing the use of the original mask annotations as pseudo-labels for the newly generated images.

Additionally, to adapt to new classes’ novel visual concepts during incremental steps, we plug in the class-wise token embedding when updating the dual-generator, thereby preserving knowledge in the pre-trained model and mitigating forgetting by avoiding entire model weights update. Moreover, to maximize the utilization of old class information, we assign pseudo-labels to the background of new step images for updating segmentation model. This strategy improves the discrimination between old and novel classes, ultimately resulting in a more accurate segmentation model. We validate the effectiveness of DiffusePast through extensive experiments on standard CISS benchmarks [31]. In summary, the main contributions of our work are as follows:

- We introduce the DiffusePast framework for CISS, which incorporates a diffusion-based generative replay module for generating and replaying semantically accurate samples. This dual-generator paradigm generates distribution-aligned and structure-preserved images, resulting in improved mask annotations and enhanced segmentation performance.
- We incorporate class-wise token embedding for continuous adaptation of dual-generator to novel visual concepts of newly added classes, and background pseudo-labeling for updating the segmentation model, which facilitates learning new knowledge while alleviating forgetting old knowledge.
- Extensive experiments demonstrate the effectiveness of our method across mainstream benchmarks, showcasing its ability to achieve a better trade-off between the old and novel classes’ performance.

2 Related work

Class incremental semantic segmentation Most CISS methods fall into two categories: regularization-based methods [6, 12, 31, 2, 46, 47, 33, 29] and replay-based methods [7, 31]. Regularization-based methods aim to preserve old class knowledge using calibrated loss functions, mitigating background shift (i.e., old class pixels in the current step images are labeled as background) and forgetting problems. For example, ALIFE [31] improves the commonly used calibrated cross-entropy and calibrated knowledge distillation losses [6] by introducing the ALI loss, which better

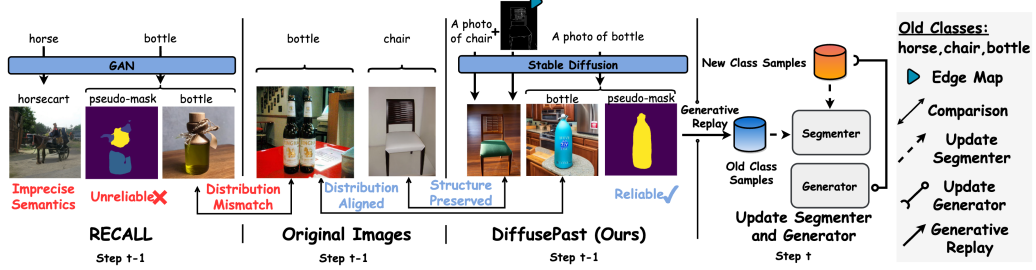


Figure 1: GAN-based generative replay method (RECALL [26]) generates inaccurate results; Our DiffusePast, leveraging Stable Diffusion [36], generates semantic accurate images of previous steps guided by *text prompts* and *edge maps*. The generated images are distribution-aligned and structure-preserved, which further results in improved masks and benefits CISS task.

preserves old class semantics in the background area, while PLOP [12] explicitly uses pseudo-labels from the old model’s predictions to address background shift. Our method combines the advantages of these approaches to incrementally update the segmentation model through both calibration and pseudo-labeling. Replay-based methods [7, 2, 44, 50] maintain a small set of samples for each old class to mitigate catastrophic forgetting and improve generalization. However, the classical memory-based approach raises privacy concerns [8, 10] and may lack diversity. On the other hand, the generative replay technique, as presented in RECALL [26], generates replayed samples using a pre-trained GAN. However, the generated images suffer from semantic imprecision and encounter out-of-distribution issues, leading to inferior mask annotations and overall performance degradation. As an alternative to using real images, ALIFE [31] proposes replaying class-wise feature embeddings, but it requires additional time-consuming steps to compensate for feature drift when new classes are introduced. Our approach differs from the previous methods in two ways:(1) We generate precise and diverse images directly from text prompts, surpassing ALIFE in obtaining richer class-wise semantics without additional modules or time-consuming feature drift compensation; (2) We continually update the generator by only optimize and store a set of class-wise embeddings, offering greater flexibility compared to the frozen generators in RECALL [26].

Synthetic data with generative models Synthetic data provides a practical solution for generating large, labeled datasets in vision tasks. These tasks include image classification [19, 1], object detection [43, 30, 16], semantic segmentation [3, 9, 23]. GANs-based methods [4, 18, 23] have been widely employed in this area. Recently, there has been increasing interest in using large-scale text-to-image diffusion models such as DALL-E 2 [35], Imagen [37], and Stable Diffusion [36]. Some works [25, 42] have explored the use of diffusion models to enhance training data for semantic segmentation tasks by leveraging cross-attention maps and fine-tuning. However, these approaches still face challenges related to sequential forgetting [39], which motivates the need for our work.

3 Method

3.1 Problem definition

During the process of training a Continual Image Semantic Segmentation (CISS) model, we utilize a series of training datasets, denoted as \mathcal{D}_t , where $t \in \{1, \dots, T\}$ refers to a specific incremental step and T represents the total number of steps. For each incremental step t , \mathcal{D}_t consists of pairs comprising an image $\mathbf{x}_t \in \mathcal{X}$ and its corresponding ground-truth masks $\mathbf{y}_t \in \mathcal{Y}_t$. For any sample pairs, $\mathbf{x}_t = \{\mathbf{x}_{t,i}\}_{i=1}^N$ and $\mathbf{y}_t = \{\mathbf{y}_{t,i}\}_{i=1}^N$ represent the N pixels of an image and its corresponding mask, respectively. The label space $\mathcal{Y}_t = \{c_b\} \cup \mathcal{C}_t$ consists of the background class c_b and a set of novel classes \mathcal{C}_t , indicating that the masks are labeled only for pixels belonging to categories in \mathcal{C}_t , while the remaining pixels are simply labeled as the background c_b . As a result, the background area of an image \mathbf{x}_t comprises a collection of pixels denoted by $\mathcal{A}_b^t = \{i | \mathbf{y}_{t,i} = c_b\}$. The pixels may actually represent objects from the old classes $\mathcal{C}_{1:t-1}$, the future classes $\mathcal{C}_{t+1:T}$, or the authentic background itself. In accordance with the prevalent assumption in CISS literature [2, 6, 7, 31], the class sets for each step are considered to be disjoint (i.e., $\mathcal{C}_{1:t-1} \cap \mathcal{C}_t = \emptyset$).

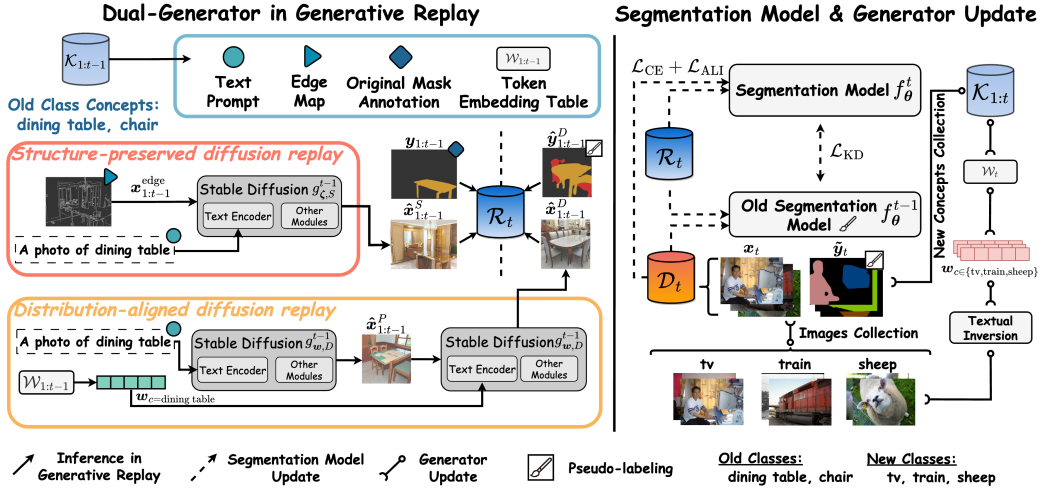


Figure 2: DiffusePast involves two stages: Inference stage including (1) **Generative replay** that generates images with reliable masks for replay via dual-generator $g_{\{\zeta, w\}}^{t-1}$. Training stage including (2) **Segmentation model update** that updates the segmentation model using the new data \mathcal{D}_t , replayed samples \mathcal{R}_t , and distilled knowledge from old segmentation model f_{θ}^{t-1} ; and (3) **Generator update** that updates the dual-generator as $g_{\{\zeta, w\}}^t$ by collecting and learning novel visual concept from \mathcal{D}_t . The old model f_{θ}^{t-1} also provides labels for images generated by the distribution-aligned diffusion replay module and assigns labels to background pixels in images of new dataset \mathcal{D}_t .

The goal of CISS is to develop a model f_{θ}^t that can identify all previously learned classes. Specifically, at step t , f_{θ}^t determines if a pixel is related to any of the known classes: $f_{\theta}^t : \mathcal{X} \rightarrow \mathbb{R}^{N \times |\mathcal{Y}_{1:t}|}$, where $\mathcal{Y}_{1:t} = \{c_b\} \cup \mathcal{C}_{1:t}$. Following previous works [31, 7], f_{θ}^t is constructed as a fully-convolutional network. It consists of a convolutional feature extraction module and a classifier for classifying the classes in $\mathcal{Y}_{1:t}$. After finishing t learning steps, the prediction for pixel i is allocated to the possible categories encountered so far, denoted as $\hat{y}_{t,i} = \arg \max_{c \in \mathcal{Y}_{1:t}} f_{\theta,c}^t(\mathbf{x}_{t,i})$.

3.2 Overview of the DiffusePast

Our objective is to find a novel and continuous way for replaying images with reliable masks that serve as knowledge of old classes, enabling the update of the segmentation model in a privacy-preserving way and mitigating the problem of catastrophic forgetting. To achieve these objectives, we introduce DiffusePast, a generative replay-based framework. The learning process of DiffusePast involves two stages as shown in Figure 2. The pseudo-code of the whole learning procedure is summarized in the supplementary material. Next, we will provide a detailed description of the two stages:

Generative replay. Generative replay aims to generate samples $\mathcal{G}_{1:t-1}$ of old classes for updating the current step segmentation model and preventing forgetting. To address semantic imprecision and distribution mismatch in existing generative replay frameworks [26], we propose a dual-generator $g_{\{\zeta, w\}}^{t-1} = \{g_{\zeta,S}^{t-1}, g_{w,D}^{t-1}\}$ that leverages pre-trained text-to-image generation models to generate accurate semantic images with text prompt as well as other concepts (e.g., edge map or class-wise token embedding) of old classes $c \in \mathcal{C}_{1:t-1}$. Specifically, the **Structure-preserved** generator $g_{\zeta,S}^{t-1}$ aims to generate images $\hat{x}_{1:t-1}^S$ that preserve the semantic layout, utilizing the text prompt and the structure indicator (i.e., edge map $x_{1:t-1}^{edge}$ derived from the old step images $\mathbf{x}_{1:t-1}$), while corresponding masks are obtained by reusing the original masks $\mathbf{y}_{1:t-1}$. The **Distribution-aligned** generator $g_{w,D}^{t-1}$ aims to generate images $\hat{x}_{1:t-1}^D$ that lie in the distribution of downstream datasets, utilizing the text prompt and class-specific token embedding $w_c \in \mathcal{W}_{1:t-1}$ while corresponding masks $\hat{y}_{1:t-1}^D$ is obtained by pseudo-labeling from old segmentation model f_{θ}^{t-1} . The improved images and more reliable masks together benefit the current step segmentation learning (See Section 3.3 for detailed information on

the two generators). Lastly, the generated samples $\mathcal{G}_{1:t-1}$, consisting of pairs of images and masks $\{\hat{\mathbf{x}}_{1:t-1}^S, \mathbf{y}_{1:t-1}; \hat{\mathbf{x}}_{1:t-1}^D, \hat{\mathbf{y}}_{1:t-1}^D\}$, are merged to form the current step replay data \mathcal{R}_t .

Segmentation model and generator update. The replayed samples \mathcal{R}_t of old classes generated in the first stage, and the training set \mathcal{D}_t can be directly used to update the current step’s segmentation model f_θ^t . Additionally, these data can be fed into the old segmentation model f_θ^{t-1} , whose output logits can be viewed as distilled knowledge and served as another supervision signal for f_θ^t (See Section 3.4 for detailed information on the loss functions). The dual-generator is updated to gain an understanding of novel visual concepts of new classes while preserving the abundant semantic space of the pre-trained generator. Specifically, for structure-preserved generator $g_{\zeta,S}^{t-1}$, we update at the *data-level* by collecting the edge maps and the masks $\{\mathbf{x}_t^{\text{edge}}, \mathbf{y}_t\}$ based on the current step dataset \mathcal{D}_t . For distribution-aligned generator $g_{w,D}^{t-1}$, we update at the *embedding-level* by learning token embeddings \mathbf{w}_c that encode the visual concept of each new class $c \in \mathcal{C}_t$. The above collected concept including the edge map, original masks, class-wise token embedding table, as well as text prompt of new classes, denoted by $\{\mathbf{x}_t^{\text{edge}}, \mathbf{y}_t, \mathcal{W}_t, \mathbf{p}_t\}$, respectively, are stored and updated from $\mathcal{K}_{1:t-1}$ to $\mathcal{K}_{1:t}$, and utilized for inference stage in the next step.

3.3 Dreaming past with diffusion

We built a dual-generator upon Stable Diffusion [36] pre-trained on large-scale image-text pairs, to generate semantically accurate images. Based on this capability, we develop two generators namely the *Structure-preserved Diffusion Replay* and the *Distribution-aligned Diffusion Replay*.

Structure-preserved diffusion replay. To generate images that maintain the semantic structure and layout of the original images $\mathbf{x}_{1:t-1}$, an intuitive approach is to utilize their masks $\mathbf{y}_{1:t-1}$ as a guide for image generation. While some existing generation models have demonstrated the ability to convert mask annotations into images [41], the inconsistencies in label semantics pose challenges when transferring pre-trained models to downstream datasets.

As a remedy, we utilize the collected edge maps $\mathbf{x}_{1:t-1}^{\text{edge}}$ (produced from old class images $\mathbf{x}_{1:t-1}$ by Canny edge detector [5]), and text prompts $\mathbf{p}_{1:t-1}$ of the old classes as conditions to synthesize images. Formally, given diffusion time step $\tau \in [0, 1]$, initial random noise $\hat{\mathbf{x}}_{\tau=1}^S \sim \mathcal{N}(0, 1)$, fixed variance schedule β_τ , and conditions $\mathbf{c} = \{\mathbf{p}_{1:t-1}, \mathbf{x}_{1:t-1}^{\text{edge}}\}$, the structure-preserved old class images $\hat{\mathbf{x}}_{1:t-1, \tau=0}^S$ can be generated by iteratively applying the reverse diffusion process (e.g., DDIM [40]):

$$\hat{\mathbf{x}}_{\tau-1}^S = \frac{\sqrt{\alpha_{\tau-1}} \mathbf{x}_t - \sqrt{\alpha_{\tau-1}(1-\alpha_{\tau})} \epsilon_\phi(\hat{\mathbf{x}}_\tau^S, \tau, \mathbf{c})}{\sqrt{\alpha_{\tau-1}\alpha_\tau}} + \sqrt{1-\alpha_{\tau-1}} \epsilon_\phi(\hat{\mathbf{x}}_\tau^S, \tau, \mathbf{c}) \quad (1)$$

where $\alpha_\tau := \prod_{s=0}^{\tau} (1 - \beta_s)$, ϵ_ϕ is the pre-trained denoising network. In practice, we utilize ControlNet [45] equipped with Stable Diffusion as the pre-trained denoising network, which supports the canny edge map as the conditions for image generation. Since synthesized images preserve the spatial consistency of original images (See qualitative results in Figure 5), thus it is reasonable to pair it with the original masks and construct the samples $\mathcal{G}_{1:t-1}^S = \{\tilde{\mathbf{x}}_{1:t-1}^S, \mathbf{y}_{1:t-1}\}$ for replay. Lastly, we add the edge map $\mathbf{x}_t^{\text{edge}}$, current step masks \mathbf{y}_t , as well as text prompt \mathbf{p}_t to $\mathcal{W}_{1:t}$ for next step inference.

Distribution-aligned diffusion replay. To generate images that preserve the diversity and align with the distribution of the downstream datasets, we follow the image-to-image translation process in [27], dividing the generation process into two sub-steps. Firstly, we generate diverse images $\hat{\mathbf{x}}_{1:t-1}^P$ based on old class text prompts $\mathbf{p}_{1:t-1}$ from scratch, and then we perform the distribution transfer on $\hat{\mathbf{x}}_{1:t-1}^P$ via class-wise token embeddings $\mathcal{W}_{1:t-1}$ of the old classes $c \in \mathcal{C}_{1:t-1}$. Formally, we first add the noise $\epsilon \sim \mathcal{N}(0, 1)$ to obtain the noised images of $\hat{\mathbf{x}}_{1:t-1}^P$ by:

$$\hat{\mathbf{x}}_{\tau=1}^P = \sqrt{\alpha_\tau} \hat{\mathbf{x}}_{\tau=0}^P + \sqrt{1-\alpha_\tau} \epsilon \quad (2)$$

where τ and α share the same definition in Eq.1. Then, we perform the reverse diffusion $\hat{\mathbf{x}}_{\tau=1}^P \rightarrow \hat{\mathbf{x}}_{\tau=0}^D$ by iterating Eq.1 with conditions $\mathbf{c} = \mathcal{W}_{1:t-1}$. The labels for generated images will be given by the old segmentation model via pseudo-labeling $\hat{\mathbf{y}}_{1:t-1,i}^D = \arg \max_{c \in \mathcal{Y}_{1:t-1}} f_{\theta,c}^{t-1}(\hat{\mathbf{x}}_{1:t-1,i}^D)$ for each pixel i . Finally, we construct the samples $\mathcal{G}_{1:t-1}^D = \{\hat{\mathbf{x}}_{1:t-1}^D, \hat{\mathbf{y}}_{1:t-1}^D\}$ for replay.

To update the generator, we learn the token embeddings $\mathbf{w}_c \in \mathcal{W}_t$ of each new class $c \in \mathcal{C}_t$ leveraging the technique of Textural Inversion [15]. Formally, we add $|\mathcal{C}_t|$ new tokens to the text vocabulary of Stable Diffusion for each new class and fine-tune these embeddings \mathbf{w}_c using the diffusion loss:

$$\mathcal{L}_{\text{token}}(\mathbf{w}_c)_{c \in \mathcal{C}_t} = \mathbb{E} [\|\epsilon - \epsilon_\phi(\mathbf{x}_{c,\tau}, \tau)\|^2] \quad (3)$$

where training image $\mathbf{x}_{c,\tau=0}$ is collected for each class $c \in \mathcal{C}_t$ with few-shot (e.g., 4) samples. Lastly, we add the learned token embeddings to $\mathcal{W}_{1:t}$. Since the optimization of each class-related token is independent and not disrupting the pretrained weights of Stable Diffusion, it does not face the forgetting problem.

3.4 Training

The optimization of the segmentation model f_θ^{t-1} based on three losses. These include the Cross-Entropy (CE) loss and ALI loss [31] for learning from generative replay samples \mathcal{R}_t and current step samples \mathcal{D}_t , and knowledge distillation (KD) loss for learning from the old segmentation model. Nevertheless, the majority of existing works [7, 31] use CE loss to learn the discrimination boundary solely based on labels of new classes $c \in \mathcal{C}_t$, overlooking the old class pixels in the background area. Motivated by [12], we aim to improve the discrimination by applying CE loss on both the ground-truth $\mathcal{A}_{\text{new}}^t = \{i | \mathbf{y}_{t,i} \in \mathcal{C}_t\}$ and pseudo-labeled areas $\mathcal{A}_{\text{old}}^t = \{i | (\mathbf{y}_{t,i} = c_b) \wedge (\hat{\mathbf{y}}_{t,i} \in \mathcal{C}_{1:t-1}) \wedge (\mu_i > \tau)\}$, where predictions $\hat{\mathbf{y}}_{t,i} = \arg \max_{c \in \mathcal{Y}_{1:t-1}} f_{\theta,c}^{t-1}(\mathbf{x}_{t,i})$ are assigned to the background pixels $\mathcal{A}_b^t = \{i | \mathbf{y}_{t,i} = c_b\}$ only when the predictions correspond to old class objects are confident. Finally, the overall objective is:

$$\mathcal{L}(i) = \lambda_{\text{CE}} \mathcal{L}_{\text{CE}}(i) \mathbb{1}[i \in \mathcal{A}_{\text{new}}^t \cup \mathcal{A}_{\text{old}}^t] + \lambda_{\text{ALI}} \mathcal{L}_{\text{ALI}}(i) \mathbb{1}[i \in \mathcal{A}_b^t] + \lambda_{\text{KD}} \mathcal{L}_{\text{KD}}(i), \quad (4)$$

where λ_{CE} , λ_{ALI} and λ_{KD} are balance parameters. \mathcal{L}_{KD} calculates the dot-product distance between the old and new segmentation model's output probabilities, while \mathcal{L}_{ALI} is the distance between the maximum logit value and the weighted average of old class logits [31].

4 Experiments

4.1 Experimental setting

Datasets and evaluation. We start by evaluating our method on the PASCAL-VOC 2012 [13] and ADE20K [48] datasets. The Pascal-VOC 2012 dataset covers 20 object and background classes. The ADE20K dataset contains 150 object and stuff classes (See supplementary material for more details of datasets). We investigated a variety of incremental learning scenarios for each dataset following the common practice [6, 7, 31]. The incremental scenario is denoted by N_b - N_n (T steps), where N_b and N_n represent the number of base and novel classes to be trained, respectively. For instance, an incremental scenario of 15-1 (6 steps) would involve learning 15 base classes first, followed by sequentially adding one novel class, requiring a total of 6 training steps. Following [31, 7], we focus on the *overlapped* setting, where unlabeled regions could contain either previous or future categories, as it is more practical in real-world applications. In line with [6, 12, 29, 7], we evaluate our method and all baselines using the mIoU_b, mIoU_n, and mIoU_{all} scores, which represent the average intersection-over-union (IoU) scores for base, novel, and all categories, respectively. We also provide the harmonic mean (hIoU) of mIoU_b and mIoU_n scores, which is less affected by the imbalance between base and novel classes.

Implementation details. We use DeepLab-V3 with ImageNet pre-trained ResNet-101 as the segmentation model, following [6, 7, 12, 31]. We employ the Stable Diffusion [36] to generate images conditioned on text prompts, and utilize the ControlNet [45] to control the Stable Diffusion, allowing for edge map conditions. We optimize the network using SGD with an initial learning rate of 1e-2 for the base stage and 1e-3 for the incremental stages. During the base stage ($t = 1$), DeepLab-V3 is trained for 30 epochs on PASCAL VOC and 60 epochs on ADE20K. For each subsequent incremental stage ($t > 1$), the number of epochs for PASCAL VOC is determined by cross-validation, while ADE20K is trained for a fixed 60 epochs, as in [31]. The batch size is set to 24 on both datasets. We use the poly schedule for adjusting the learning rate. We follow the learning rate schedule, data augmentation, and output stride outlined in [31] for all experiments. The replayed sample size is set as 100 for Pascal VOC and 300 for ADE20K, following [7]. The experiments were conducted using PyTorch 1.13.1 [32] on two NVIDIA A100 GPUs. We report IoU scores averaged over 3 runs. A detailed description of hyperparameter settings can be found in the supplementary material.

4.2 Experimental results on benchmark datasets

Table 1: Experimental results on PASCAL-VOC [13]. ALIFE-M uses feature replay, while RECALL uses generative replay. Note that RECALL [26] generates 500 samples for each old class. Numbers in bold are the best performance, while underlined ones are the second best. Numbers for other methods are taken from ALIFE [31].

| Methods | 19-1 (2 steps) | | | | 15-5 (2 steps) | | | | 15-1 (6 steps) | | | |
|--------------------------------------|----------------|------------|--------------|--------------|----------------|------------|--------------|--------------|----------------|------------|--------------|--------------|
| | 0-19 | 20 | mIoU | hIoU | 0-15 | 16-20 | mIoU | hIoU | 0-15 | 16-20 | mIoU | hIoU |
| EWC [22] | 26.90 | 14.00 | 26.30 | 18.42 | 24.30 | 35.50 | 27.10 | 28.85 | 0.30 | 4.30 | 1.30 | 0.56 |
| LwF-MC [24] | 64.40 | 13.30 | 61.90 | 22.05 | 58.10 | 35.00 | 52.30 | 43.68 | 6.40 | 8.40 | 6.90 | 7.26 |
| ILT [28] | 67.75 | 10.88 | 65.05 | 18.75 | 67.08 | 39.23 | 60.45 | 49.51 | 8.75 | 7.99 | 8.56 | 8.35 |
| MiB [6] | 70.42 | 17.70 | 67.91 | 28.25 | 76.68 | 49.03 | 70.09 | 59.81 | 37.98 | 12.28 | 31.86 | 18.56 |
| SDR [29] | 71.30 | 23.40 | 69.00 | 35.24 | 76.30 | 50.20 | 70.10 | 60.56 | 47.30 | 14.70 | 39.50 | 22.43 |
| PLOP [12] | 75.89 | 34.90 | 73.94 | 47.81 | 76.37 | 49.55 | 69.98 | 60.10 | 64.51 | 19.93 | 53.90 | 30.45 |
| SSUL [7] | 77.73 | 29.68 | 75.44 | 42.96 | 77.82 | 50.10 | 71.22 | 60.96 | 77.31 | 36.59 | 67.61 | 49.67 |
| ALIFE [31] | 76.61 | 49.36 | 75.31 | 60.03 | 77.18 | 52.52 | 71.31 | 62.50 | 64.44 | 34.91 | 57.41 | 45.29 |
| Ours-\mathcal{L} | 77.59 | 54.00 | 75.51 | 63.35 | 78.05 | 53.13 | 72.10 | 63.22 | 63.94 | 36.64 | 57.44 | 46.58 |
| Ours | ± 0.01 | ± 0.00 | 75.51 | 63.35 | ± 0.02 | ± 0.03 | 72.10 | 63.22 | ± 0.10 | ± 0.04 | ± 0.53 | ± 0.21 |
| ALIFE-M [31] | 76.72 | 52.29 | <u>75.56</u> | <u>62.19</u> | 77.66 | 55.27 | <u>72.33</u> | <u>64.57</u> | 66.09 | 38.81 | 59.59 | 48.89 |
| RECALL [26] | 68.10 | 55.30 | 68.60 | 61.04 | 67.70 | 54.30 | 65.60 | 60.26 | 67.80 | 50.90 | <u>64.80</u> | <u>58.15</u> |
| Ours-DiffusePast | 76.75 | 57.16 | 75.82 | 65.52 | 78.47 | 57.36 | 73.45 | 66.27 | 74.68 | 49.17 | 68.60 | 59.30 |
| | ± 0.04 | ± 0.04 | ± 0.04 | ± 0.04 | ± 0.01 | ± 0.04 | ± 0.01 | ± 0.03 | ± 0.17 | ± 0.25 | ± 0.18 | ± 0.22 |

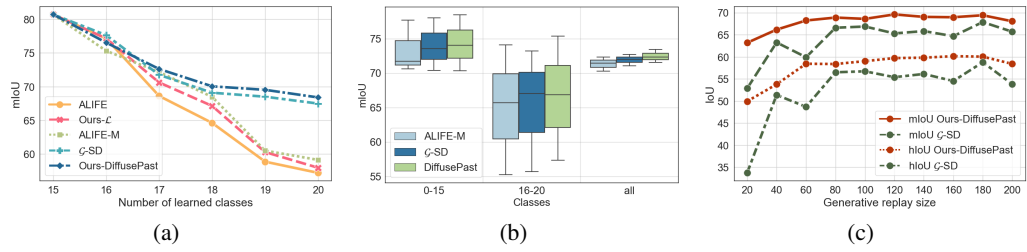


Figure 3: (a): mIoU evaluation on VOC 15-1, (b): Comparison of mIoU distribution for three different class-orderings on VOC 15-5, (c): mIoU and hIoU on VOC 15-1 with varying replay size.

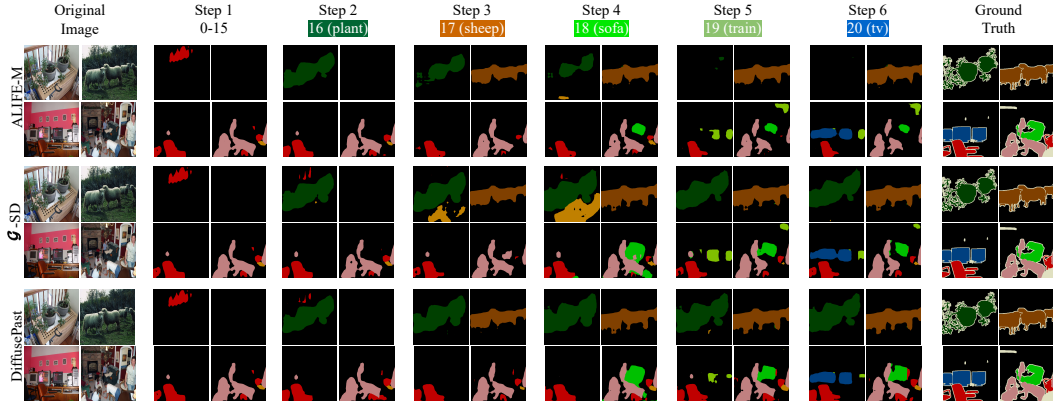


Figure 4: Qualitative results on VOC 15-1 scenario.

PASCAL VOC. We compare our approach in Table 1 with state-of-the-art CISS methods, including regularization-based methods [31, 7, 6, 12] and replay-based methods that do not use real images [31, 26]. We have the following observations: (1) The proposed loss, Ours- \mathcal{L} , outperforms all other methods without replay (especially ALIFE, which also uses ALI loss) in 19-1 and 15-5 scenarios. This highlights the effectiveness of utilizing old class knowledge in the cross-entropy loss. Note that a comparison of SSUL [7] is not fair due to its use of a saliency detector that allows more

classes (i.e., future objects) for discrimination learning on 15-1. (2) Replay strategies without real images (ALIFE-M, RECALL, and DiffusePast) effectively consolidate old class knowledge and enhance novel class learning. This validates the intuition that by involving old pixels, the model learns with more information, resulting in improved discrimination boundaries. (3) Our proposed DiffusePast, utilizing diffusion-based generative replay, outperforms other replay-based methods with significant improvements (the largest mIoU gains of 3.80% on 15-1 and hIoU gains of 3.33% on 19-1), and achieve substantial gains over Ours- \mathcal{L} (the largest mIoU and hIoU gains of 11.16% and 12.72% on 15-1). These results confirm the effectiveness of our approach.

To further analyze the more challenging tasks 15-1, we show the mIoU evolution at each incremental step in Figure 3(a). The results show that the proposed loss function (Ours- \mathcal{L}) consistently outperforms ALIFE at every step and even matches the performance of ALIFE-M. These results indicate that the properly utilized pseudo-labels are effective for CISS. Besides, we found that generative replay-based methods (DiffusePast and \mathcal{G} -SD) achieve substantial increases in mIoU when new classes are incrementally learned. Moreover, compared to \mathcal{G} -SD, which replays images generated by vanilla Stable Diffusion, DiffusePast consistently achieves better performance when $t \geq 3$. These results validate the effectiveness of the proposed dual-generator and confirm the intuition that improved images and reliable masks benefit the final performance. We also evaluate the performance robustness of DiffusePast on different class orderings in VOC 15-5. Figure 3(b) shows that DiffusePast consistently achieves higher mIoUs than other methods, demonstrating its robustness.



Figure 5: Visualization of generated images on VOC 15-1 at last four incremental steps with GAN, Stable-Diffusion (SD), Structure-preserved Diffusion Replay (SDR), and Distribution-aligned Diffusion Replay (DDR). *pottedplant*, *sheep*, *sofa* and *train* are generated samples for replay.

Qualitative results. Figure 4 shows a qualitative analysis of our approach compared to other replay-based methods (ALIFE-M and \mathcal{G} -SD), showcasing results for four images per learning step in the VOC 15-1 task. These images contain the newly learned classes $\{plant, sheep, sofa, train, tv\}$ as well as old classes $\{person, chair\}$. Our DiffusePast exhibits both less forgetting and better new class learning based on the following observations: First, unlike ALIFE-M, the generative-replay based methods preserve the knowledge of base step classes (e.g., *person* and *chair*) and intermediate step classes (e.g., *plant*). Further, DiffusePast retain more old class knowledge (e.g., *person*) from the base steps compared with \mathcal{G} -SD; Second, we observe that both \mathcal{G} -SD and DiffusePast effectively learn new classes (e.g., *sheep*). In addition, DiffusePast effectively mitigates the false-positive predictions (e.g., predicted *sofa* near the *tv* in Step 5). We also compare the old class images produced by different generative-replay strategies. Figure 5 shows that the images generated by distribution-aligned diffusion replay (DDR) more closely match the original data than GAN and SD, while the structure-preserved diffusion replay (SDR) generates images with layouts similar to the original

Table 2: Experimental results on ADE20K [48]. Numbers in bold are the best performance, while underlined ones are the second best. Numbers for other methods are taken from ALIFE [31].

| Methods | 100-50 (2 steps) | | | | 50-50 (3 steps) | | | | 100-10 (6 steps) | | | |
|--------------------------------------|------------------|------------|--------------|--------------|-----------------|------------|--------------|--------------|------------------|------------|--------------|--------------|
| | 0-100 | 101-150 | mIoU | hIoU | 0-50 | 51-150 | mIoU | hIoU | 0-100 | 101-150 | mIoU | hIoU |
| ILT [28] | 18.29 | 14.40 | 17.00 | 16.11 | 3.53 | 12.85 | 9.70 | 5.54 | 0.08 | 1.31 | 0.49 | 0.15 |
| MiB [6] | 40.52 | 17.17 | 32.79 | 24.12 | 45.57 | 21.01 | 29.31 | 28.76 | 38.21 | 11.12 | 29.24 | 17.23 |
| PLOP [12] | 42.10 | 16.22 | 33.53 | 23.42 | 48.24 | 21.31 | 30.40 | 29.56 | 40.78 | 14.02 | 31.92 | 20.87 |
| SSUL [7] | 41.28 | 18.02 | 33.58 | 25.09 | 48.38 | 20.15 | 29.56 | 28.45 | 40.20 | 18.75 | 33.10 | 25.57 |
| ALIFE [31] | 42.18 | 23.07 | <u>35.86</u> | <u>29.83</u> | 48.98 | 25.69 | <u>33.56</u> | <u>33.70</u> | 41.02 | 22.76 | <u>34.98</u> | 29.28 |
| Ours-\mathcal{L} | 42.12 | 24.87 | 36.41 | 31.28 | 48.78 | 28.92 | 35.62 | 36.31 | 41.66 | 22.20 | 35.21 | 28.96 |
| | ± 0.00 | ± 0.02 | ± 0.01 | ± 0.02 | ± 0.00 | ± 0.01 | ± 0.01 | ± 0.01 | ± 0.23 | ± 0.16 | ± 0.11 | ± 0.07 |
| ALIFE-M [31] | 42.28 | 23.58 | <u>36.09</u> | <u>30.28</u> | 48.99 | 26.15 | <u>33.87</u> | <u>34.10</u> | 41.17 | 23.07 | <u>35.18</u> | <u>29.57</u> |
| Ours-DiffusePast | 42.26 | 24.86 | 36.50 | 31.31 | 48.93 | 29.13 | 35.82 | 36.52 | 41.76 | 23.85 | 35.83 | 30.36 |
| | ± 0.02 | ± 0.04 | ± 0.00 | ± 0.02 | ± 0.01 | ± 0.04 | ± 0.02 | ± 0.02 | ± 0.04 | ± 0.18 | ± 0.03 | ± 0.13 |

images, validating the rationale of reusing the original masks. These improvements validate the effectiveness of the proposed dual-generator and contribute to the overall performance enhancement.

ADE20K. Table 2 presents quantitative results on ADE20K, a densely labeled dataset with rich semantics in the background area at each incremental step. Note that RECALL [26] is not designed to handle stuff categories, thus results are not available. Similar to the observations in VOC, the results again demonstrate the effectiveness of Ours- \mathcal{L} and Ours-DiffusePast for densely labeled datasets. The qualitative results on ADE20K can be found in the supplementary material.

4.3 Discussion

Ablation study on generator. Table 3 presents the effect of each generator in DiffusePast on VOC 15-5 and ADE20K 50-50. The last four lines in the tables compare the performance between different generation paradigms. The results show that SDR and DDR perform better than SD on VOC 15-5, while DDR outperforms SD on ADE20K 50-50. This performance degradation of SDR on ADE20K may attribute to the difficulty of generating high-quality images on complex scenes. As a result, our DiffusePast merges the samples with a ratio of 0.8 for DDR and achieves better performance on VOC 15-5 while using DDR-generated samples directly on ADE20K 50-50. We also compare the results with memory replay-based methods. The first two lines in the table show that our DiffusePast outperforms SSUL-M and Ours-M (Ours- \mathcal{L} equipped with memory-replay) in both scenarios. A plausible reason is that the frozen feature extractor in SSUL-M limits its adaptability to new class knowledge. Another reason may be that our DiffusePast generates diverse old class samples at each step, providing more knowledge compared to fixed memory replay.

Ablation study on loss function. Table 4 presents an ablation analysis of Ours- \mathcal{L} (Eq. 4). The first row shows that using the KD on the *bg* logit results in degraded performance. This is because the old segmentation model tends to assign low probabilities to new classes, and distilling such logit will interfere with the learning of new classes. The second and third rows highlight the effectiveness of the pseudo-labels strategy, which mitigates forgetting and enhances discrimination for both old and new classes. The remaining rows present the same observations when using the generative replay \mathcal{G} .

Table 3: Ablation study for generative replay \mathcal{G} with Stable-Diffusion (SD), Structure-preserved Diffusion Replay (SDR), and Distribution-aligned Diffusion Replay (DDR) on VOC 15-5 and ADE20K 50-50. Memory replay-based methods (SSUL-M, Ours-M) are also included for comparison.

| Methods | 15-5 (2 steps) | | | | 50-50 (3 steps) | | | |
|---------------------|----------------|-------|--------------|--------------|-----------------|--------|--------------|--------------|
| | 0-15 | 16-20 | mIoU | hIoU | 0-50 | 51-150 | mIoU | hIoU |
| SSUL-M [7] | 78.40 | 55.80 | 73.02 | 65.20 | 49.12 | 20.10 | 29.77 | 28.53 |
| Ours-M | 77.83 | 55.26 | 72.46 | 64.63 | 48.71 | 29.00 | 35.66 | 36.36 |
| \mathcal{G} - SD | 78.02 | 55.77 | 72.72 | 65.04 | 48.77 | 28.84 | 35.57 | 36.25 |
| \mathcal{G} - SDR | 77.92 | 56.92 | 72.92 | 65.79 | 48.86 | 28.77 | 35.56 | 36.22 |
| \mathcal{G} - DDR | 78.45 | 56.58 | 73.24 | 65.74 | 48.93 | 29.13 | 35.82 | 36.52 |
| DiffusePast | 78.47 | 57.36 | 73.45 | 66.27 | 48.93 | 29.13 | 35.82 | 36.52 |

Table 4: Comparison of IoU scores using different loss terms on VOC 15-5. *Pseudo* indicates that CE is applied on pseudo-labeled regions. *bg* logit indicates that KD is applied on both old class logits and the *bg* logit.

| Ground-truth | Pseudo | bg logit | CE | KD | \mathcal{G} | 0-15 | 16-20 | mIoU | hIoU |
|--------------|--------|----------|----|----|---------------|-------|-------|--------------|--------------|
| | | | | | | | | | |
| ✓ | | | ✓ | | | 76.96 | 51.22 | 70.83 | 61.52 |
| ✓ | | | | ✓ | | 78.00 | 52.93 | 72.03 | 63.07 |
| ✓ | ✓ | | | | | 78.05 | 53.13 | 72.10 | 63.22 |
| ✓ | | ✓ | | ✓ | | 78.13 | 56.40 | 72.96 | 65.51 |
| ✓ | | | ✓ | | | 78.30 | 57.22 | 73.28 | 66.12 |
| ✓ | ✓ | ✓ | ✓ | ✓ | | 78.47 | 57.36 | 73.45 | 66.27 |

Generative replay size. Figure 3(c) shows the effect of the generative replay size. It shows that DiffusePast consistently outperforms \mathcal{G} -SD for different replay size. Also, even tiny generated samples from DiffusePast significantly contribute to increasing the mIoU and hIoU. In contrast, the small size of generated samples (e.g., 20) from Stable Diffusion even degrades the performance, which also demonstrates the problems of distribution mismatch.

5 Conclusion and limitations

We proposed a novel and adaptive generative replay-based framework for the CISS task. While our framework shows promise, it does have certain limitations. The first limitation is the increased storage requirements due to the need for additional device storage to store the generated old class samples. This can be challenging when dealing with a large number of classes. Another limitation is the slow inference speed of the text-to-image diffusion model, which hinders real-time or efficient inference when scaling up to a million classes in CISS. Despite these limitations, our framework still offers valuable contributions in addressing CISS challenges and can be effective in various scenarios.

References

- [1] Shekoofeh Azizi, Simon Kornblith, Chitwan Saharia, Mohammad Norouzi, and David J Fleet. Synthetic data from diffusion models improves imagenet classification. *arXiv preprint arXiv:2304.08466*, 2023.
- [2] Donghyeon Baek, Youngmin Oh, Sanghoon Lee, Junghyup Lee, and Bumsub Ham. Decomposed knowledge distillation for class-incremental semantic segmentation. 2022.
- [3] Dmitry Baranchuk, Ivan Rubachev, Andrey Voynov, Valentin Khrulkov, and Artem Babenko. Label-efficient semantic segmentation with diffusion models. *arXiv preprint arXiv:2112.03126*, 2021.
- [4] Andrew Brock, Jeff Donahue, and Karen Simonyan. Large scale gan training for high fidelity natural image synthesis. *arXiv preprint arXiv:1809.11096*, 2018.
- [5] John Canny. A computational approach to edge detection. *IEEE Transactions on pattern analysis and machine intelligence*, (6):679–698, 1986.
- [6] Fabio Cermelli, Massimiliano Mancini, Samuel Rota Bulo, Elisa Ricci, and Barbara Caputo. Modeling the background for incremental learning in semantic segmentation. In *Proceedings of the IEEE/CVF Conference on Computer Vision and Pattern Recognition*, pages 9233–9242, 2020.
- [7] Sungmin Cha, YoungJoon Yoo, Taesup Moon, et al. Ssul: Semantic segmentation with unknown label for exemplar-based class-incremental learning. *Advances in neural information processing systems*, 34:10919–10930, 2021.
- [8] Mahawaga Arachchige Pathum Chamikara, Peter Bertók, Dongxi Liu, Seyit Camtepe, and Ibrahim Khalil. Efficient data perturbation for privacy preserving and accurate data stream mining. *Pervasive and Mobile Computing*, 48:1–19, 2018.
- [9] Yuhua Chen, Wen Li, Xiaoran Chen, and Luc Van Gool. Learning semantic segmentation from synthetic data: A geometrically guided input-output adaptation approach. In *Proceedings of the IEEE/CVF conference on computer vision and pattern recognition*, pages 1841–1850, 2019.
- [10] Matthias De Lange, Rahaf Aljundi, Marc Masana, Sarah Parisot, Xu Jia, Aleš Leonardis, Gregory Slabaugh, and Tinne Tuytelaars. A continual learning survey: Defying forgetting in classification tasks. *IEEE transactions on pattern analysis and machine intelligence*, 44(7):3366–3385, 2021.
- [11] Jia Deng, Wei Dong, Richard Socher, Li-Jia Li, Kai Li, and Li Fei-Fei. Imagenet: A large-scale hierarchical image database. In *2009 IEEE conference on computer vision and pattern recognition*, pages 248–255. Ieee, 2009.

[12] Arthur Douillard, Yifu Chen, Arnaud Dapogny, and Matthieu Cord. Plop: Learning without forgetting for continual semantic segmentation. In *Proceedings of the IEEE/CVF Conference on Computer Vision and Pattern Recognition*, pages 4040–4050, 2021.

[13] Mark Everingham, Luc Van Gool, Christopher KI Williams, John Winn, and Andrew Zisserman. The pascal visual object classes (voc) challenge. *International journal of computer vision*, 88:303–338, 2010.

[14] Luciano Floridi and Massimo Chiriatti. Gpt-3: Its nature, scope, limits, and consequences. *Minds and Machines*, 30:681–694, 2020.

[15] Rinon Gal, Yuval Alaluf, Yuval Atzmon, Or Patashnik, Amit H Bermano, Gal Chechik, and Daniel Cohen-Or. An image is worth one word: Personalizing text-to-image generation using textual inversion. *arXiv preprint arXiv:2208.01618*, 2022.

[16] Yunhao Ge, Jiashu Xu, Brian Nlong Zhao, Laurent Itti, and Vibhav Vineet. Dall-e for detection: Language-driven context image synthesis for object detection. *arXiv preprint arXiv:2206.09592*, 2022.

[17] Ian Goodfellow, Jean Pouget-Abadie, Mehdi Mirza, Bing Xu, David Warde-Farley, Sherjil Ozair, Aaron Courville, and Yoshua Bengio. Generative adversarial networks. *Communications of the ACM*, 63(11):139–144, 2020.

[18] Sven Gowal, Sylvestre-Alvise Rebuffi, Olivia Wiles, Florian Stimberg, Dan Andrei Calian, and Timothy A Mann. Improving robustness using generated data. *Advances in Neural Information Processing Systems*, 34:4218–4233, 2021.

[19] Ruifei He, Shuyang Sun, Xin Yu, Chuhui Xue, Wenqing Zhang, Philip Torr, Song Bai, and Xiaojuan Qi. Is synthetic data from generative models ready for image recognition? *arXiv preprint arXiv:2210.07574*, 2022.

[20] Heechul Jung, Jeongwoo Ju, Minju Jung, and Junmo Kim. Less-forgetting learning in deep neural networks. *arXiv preprint arXiv:1607.00122*, 2016.

[21] Alexander Kirillov, Eric Mintun, Nikhila Ravi, Hanzi Mao, Chloe Rolland, Laura Gustafson, Tete Xiao, Spencer Whitehead, Alexander C Berg, Wan-Yen Lo, et al. Segment anything. *arXiv preprint arXiv:2304.02643*, 2023.

[22] James Kirkpatrick, Razvan Pascanu, Neil Rabinowitz, Joel Veness, Guillaume Desjardins, Andrei A Rusu, Kieran Milan, John Quan, Tiago Ramalho, Agnieszka Grabska-Barwinska, et al. Overcoming catastrophic forgetting in neural networks. *Proceedings of the national academy of sciences*, 114(13):3521–3526, 2017.

[23] Daiqing Li, Huan Ling, Seung Wook Kim, Karsten Kreis, Sanja Fidler, and Antonio Torralba. Bigdatasetgan: Synthesizing imagenet with pixel-wise annotations. In *Proceedings of the IEEE/CVF Conference on Computer Vision and Pattern Recognition*, pages 21330–21340, 2022.

[24] Zhizhong Li and Derek Hoiem. Learning without forgetting. *IEEE transactions on pattern analysis and machine intelligence*, 40(12):2935–2947, 2017.

[25] Ziyi Li, Qinye Zhou, Xiaoyun Zhang, Ya Zhang, Yanfeng Wang, and Weidi Xie. Guiding text-to-image diffusion model towards grounded generation. *arXiv preprint arXiv:2301.05221*, 2023.

[26] Andrea Maracani, Umberto Michieli, Marco Toldo, and Pietro Zanuttigh. Recall: Replay-based continual learning in semantic segmentation. In *Proceedings of the IEEE/CVF International Conference on Computer Vision*, pages 7026–7035, 2021.

[27] Chenlin Meng, Yutong He, Yang Song, Jiaming Song, Jiajun Wu, Jun-Yan Zhu, and Stefano Ermon. Sdedit: Guided image synthesis and editing with stochastic differential equations. In *International Conference on Learning Representations*, 2021.

[28] Umberto Michieli and Pietro Zanuttigh. Incremental learning techniques for semantic segmentation. In *Proceedings of the IEEE/CVF international conference on computer vision workshops*, pages 0–0, 2019.

[29] Umberto Michieli and Pietro Zanuttigh. Continual semantic segmentation via repulsion-attraction of sparse and disentangled latent representations. In *Proceedings of the IEEE/CVF conference on computer vision and pattern recognition*, pages 1114–1124, 2021.

[30] Minheng Ni, Zitong Huang, Kailai Feng, and Wangmeng Zuo. Imaginarynet: Learning object detectors without real images and annotations. *arXiv preprint arXiv:2210.06886*, 2022.

[31] Youngmin Oh, Donghyeon Baek, and Bumsub Ham. ALIFE: Adaptive logit regularizer and feature replay for incremental semantic segmentation. In Alice H. Oh, Alekh Agarwal, Danielle Belgrave, and Kyunghyun Cho, editors, *Advances in Neural Information Processing Systems*, 2022.

[32] Adam Paszke, Sam Gross, Francisco Massa, Adam Lerer, James Bradbury, Gregory Chanan, Trevor Killeen, Zeming Lin, Natalia Gimelshein, Luca Antiga, et al. Pytorch: An imperative style, high-performance deep learning library. *Advances in neural information processing systems*, 32, 2019.

[33] Minh Hieu Phan, Son Lam Phung, Long Tran-Thanh, Abdesselam Bouzerdoum, et al. Class similarity weighted knowledge distillation for continual semantic segmentation. In *Proceedings of the IEEE/CVF Conference on Computer Vision and Pattern Recognition*, pages 16866–16875, 2022.

[34] Alec Radford, Jong Wook Kim, Chris Hallacy, Aditya Ramesh, Gabriel Goh, Sandhini Agarwal, Girish Sastry, Amanda Askell, Pamela Mishkin, Jack Clark, et al. Learning transferable visual models from natural language supervision. In *International conference on machine learning*, pages 8748–8763. PMLR, 2021.

[35] Aditya Ramesh, Prafulla Dhariwal, Alex Nichol, Casey Chu, and Mark Chen. Hierarchical text-conditional image generation with clip latents. *arXiv preprint arXiv:2204.06125*, 2022.

[36] Robin Rombach, Andreas Blattmann, Dominik Lorenz, Patrick Esser, and Björn Ommer. High-resolution image synthesis with latent diffusion models. In *Proceedings of the IEEE/CVF Conference on Computer Vision and Pattern Recognition*, pages 10684–10695, 2022.

[37] Chitwan Saharia, William Chan, Saurabh Saxena, Lala Li, Jay Whang, Emily L Denton, Kamyar Ghasemipour, Raphael Gontijo Lopes, Burcu Karagol Ayan, Tim Salimans, et al. Photorealistic text-to-image diffusion models with deep language understanding. *Advances in Neural Information Processing Systems*, 35:36479–36494, 2022.

[38] Hanul Shin, Jung Kwon Lee, Jaehong Kim, and Jiwon Kim. Continual learning with deep generative replay. *Advances in neural information processing systems*, 30, 2017.

[39] James Seale Smith, Yen-Chang Hsu, Lingyu Zhang, Ting Hua, Zsolt Kira, Yilin Shen, and Hongxia Jin. Continual diffusion: Continual customization of text-to-image diffusion with c-lora. *arXiv preprint arXiv:2304.06027*, 2023.

[40] Jiaming Song, Chenlin Meng, and Stefano Ermon. Denoising diffusion implicit models. *arXiv preprint arXiv:2010.02502*, 2020.

[41] Weilun Wang, Jianmin Bao, Wengang Zhou, Dongdong Chen, Dong Chen, Lu Yuan, and Houqiang Li. Semantic image synthesis via diffusion models. *arXiv preprint arXiv:2207.00050*, 2022.

[42] Weijia Wu, Yuzhong Zhao, Mike Zheng Shou, Hong Zhou, and Chunhua Shen. Diffumask: Synthesizing images with pixel-level annotations for semantic segmentation using diffusion models. *arXiv preprint arXiv:2303.11681*, 2023.

[43] Zhenyu Wu, Lin Wang, Wei Wang, Tengfei Shi, Chenglizhao Chen, Aimin Hao, and Shuo Li. Synthetic data supervised salient object detection. In *Proceedings of the 30th ACM International Conference on Multimedia*, pages 5557–5565, 2022.

- [44] Shipeng Yan, Jiale Zhou, Jiangwei Xie, Songyang Zhang, and Xuming He. An em framework for online incremental learning of semantic segmentation. In *Proceedings of the 29th ACM international conference on multimedia*, pages 3052–3060, 2021.
- [45] Lvmin Zhang and Maneesh Agrawala. Adding conditional control to text-to-image diffusion models. *arXiv preprint arXiv:2302.05543*, 2023.
- [46] Zekang Zhang, Guangyu Gao, Zhiyuan Fang, Jianbo Jiao, and Yunchao Wei. Mining unseen classes via regional objectness: A simple baseline for incremental segmentation. *arXiv preprint arXiv:2211.06866*, 2022.
- [47] Hanbin Zhao, Fengyu Yang, Xinghe Fu, and Xi Li. Rbc: Rectifying the biased context in continual semantic segmentation. In *Computer Vision–ECCV 2022: 17th European Conference, Tel Aviv, Israel, October 23–27, 2022, Proceedings, Part XXXIV*, pages 55–72. Springer, 2022.
- [48] Bolei Zhou, Hang Zhao, Xavier Puig, Sanja Fidler, Adela Barriuso, and Antonio Torralba. Scene parsing through ade20k dataset. In *Proceedings of the IEEE conference on computer vision and pattern recognition*, pages 633–641, 2017.
- [49] Da-Wei Zhou, Qi-Wei Wang, Zhi-Hong Qi, Han-Jia Ye, De-Chuan Zhan, and Ziwei Liu. Deep class-incremental learning: A survey. *arXiv preprint arXiv:2302.03648*, 2023.
- [50] Lanyun Zhu, Tianrun Chen, Jianxiong Yin, Simon See, and Jun Liu. Continual semantic segmentation with automatic memory sample selection. *arXiv preprint arXiv:2304.05015*, 2023.